JOURNAL OF PROPULSION AND POWER
Vol. 18, No. 3, May–June 2002

Evaluation of Ultrasound Technique for Solid-Propellant Burning-Rate Response Measurements

Jeffrey J. Murphy* and Herman Krier†
University of Illinois at Urbana–Champaign, Urbana, Illinois 61801

The development of an ultrasound technique for precisely measuring the instantaneous regression rate of a solid-rocket propellant under transient conditions is reviewed. The technique is used to measure the burning-rate response of several solid propellants to an oscillatory chamber pressure with a frequency of up to 300 Hz. This measurement is known as the propellant's pressure-coupled response function and is used as an input into rocket stability prediction models. The ultrasound waveforms are analyzed using cross-correlation and other digital signal processing techniques to determine burning rate. Digital methods are less prone to bias and offer greater flexibility than other techniques previously used. The resulting data are corrected for compression effects. The effects of a changing thermal profile on the measurement are discussed. Other phenomena that may corrupt the measurement, such as surface roughness, are also covered. Results of the experiments are compared to data from two other measurement techniques: a T-burner and a magnetic flowmeter.

Nomenclature

A	=	quasi-steady gas-phase and solid-phase reaction layer, homogeneous, one-dimensional solid (QSHOD) parameter, $(\partial\dot{r}/\partial T_s)_p$
$\boldsymbol{A}$	=	amplitude, or envelope function
a_T	=	temperature shift factor
B	=	QSHOD parameter, $(\partial\dot{r}/\partial T_0)_p$
$\boldsymbol{C}$	=	group velocity
C_1, C_2	=	Williams–Landel–Ferry (see Refs. 28 and 51) constants, see Eq. (26)
c	=	phase speed
d	=	particle diameter
f	=	frequency, or arbitrary function
G	=	spectral density function, or shear modulus
g	=	arbitrary function
h	=	propellant height
i	=	$(-1)^{1/2}$
K	=	bulk modulus
k	=	wave number
M	=	bulk longitudinal modulus
n	=	QSHOD parameter, $(\partial\dot{r}/\partial p)_{T_0}$
n_s	=	QSHOD parameter, $(\partial\dot{r}/\partial p)_{T_s}$
$\boldsymbol{P}$	=	principal part
p	=	pressure
R	=	cross-correlation function
$\boldsymbol{R}$	=	response function
$\dot{r}$	=	burning rate
T	=	period, or temperature
t	=	time
u	=	particle displacement in wave equation
w	=	integration variable
x	=	distance
α	=	attenuation coefficient
Δt	=	round-trip time
Δx	=	propellant thickness
δ	=	round-trip time
$\delta\bullet$	=	experimental error
λ	=	QSHOD condensed phase eigenvalue, defined in Eq. (21)
ν	=	Poisson's ratio
ξ	=	thermal boundary-layer thickness
ρ	=	density
Ω	=	nondimensional frequency
ω	=	frequency
$\lvert\ \rvert$	=	magnitude of a complex number
$\arg\bullet$	=	phase of a complex number
$\langle\ \rangle$	=	averaged quantity

Subscripts

eff	=	effective
f	=	final value
i	=	imaginary part, or initial value
r	=	real part
s	=	surface
0	=	reference value

Accents and Superscripts

$\hat{}$	=	composite signal
$\bar{}$	=	steady-state quantity
$'$	=	unsteady quantity
$\tilde{}$	=	Hilbert transform of a signal

Received 30 March 2001; revision received 12 November 2001; accepted for publication 22 December 2001.

*Graduate Research Assistant, Department of Mechanical and Industrial Engineering, 1206 West Green Street; currently Postdoctoral Appointee, Combustion Research Facility, Sandia National Laboratories, P.O. Box 969, MS 9052, Livermore, CA 94551. Member AIAA.

†Richard W. Kritzer Distinguished Professor, Department of Mechanical and Industrial Engineering, 1206 West Green Street. Fellow AIAA.

Introduction

A TECHNIQUE for measuring transient burning rates of solid-rocket propellants using ultrasound is discussed. The technique is applied to the problem of estimating the response of the burning rate of a solid propellant to pressure oscillations. This measurement, known as the pressure-coupled response function, is needed for predicting combustion-driven instability in solid-rocket motors. The transient burning-rate response also provides experimental data for comparison with propellant combustion models.

It was only a matter of time after ultrasound pulse-echo thickness measurement techniques were developed that someone would apply the diagnostic to measure burning rates of solid fuels and propellants. As early as 1964, one can find brief references to ultrasound measurements in hybrid solid-rocket motors in Sweden.[1]

At the same time, similar techniques were being investigated at universities in the United States[2,3] and at NASA.[4] Since then, the technique has been developed mainly by researchers at ONERA,[5–8] although it has seen many uses by other researchers in the United States[9,10] and overseas.[11–14] A more thorough review of past and current applications of ultrasound burning-rate measurement techniques was recently published by Frederick and Traineau.[15]

Our work differs from that cited in that digital signal processing technology is used to analyze the ultrasound pulse-echo data. To our knowledge, no one had made wholesale use of digital signal processing for propellant burning-rate measurement before 1995, when we began this project. (Since then, researchers at ONERA reported the use of digital techniques in a study of rocket insulation behavior using ultrasound.[16]) These digital techniques offer superior signal detection compared to analog methods and are much more flexible.

Ultrasound is a well-proven technique for measuring steady-state burning rates. Transient burning rates are a different matter. One can find references to transient burning-rate measurements in the literature (e.g., Refs. 7, 8, 12, and 17–19). These papers generally include the observation that the technique does not appear to work very well for fast transients. Very little analysis has been done, however, to determine what exactly are the limits of the technique. The study published in Ref. 8 is notable in that it compares unsteady ultrasound measurments to the results of several other response measurement techniques. The major goal of this paper is to quantify some of the errors that arise when applying an ultrasound burning-rate measurement technique under transient conditions.

This paper starts with a conceptual overview of the ultrasound measurement technique. A brief discussion of physical acoustics in solids follows. Then, the measurement system is covered. The techniques for signal detection and processing are described next. Compression of the propellant caused by pressure, the thermal profile in the propellant, surface roughness, and other physical phenomena that can distort the measurements are discussed. Measurements of the pressure-coupled burning-rate response function of four propellants are presented last. Data from one of these propellants are compared with data from a magnetic flowmeter[20] and from a T-burner.[21]

Experimental Method

It is straightforward to make a simple thickness measurement using ultrasound echo location.[22] A pulse is sent into the sample to be measured by means of an ultrasonic transducer coupled to its surface. The pulse travels through the sample, reflects from the opposite surface, and returns to the transducer. The time that it took the pulse to make the trip is recorded, and the sample thickness is then determined by the formula

$$\Delta x = c\Delta t/2 \tag{1}$$

where Δx is the thickness and Δt is the measured round-trip time. The speed of sound in the material c is presumably determined from previous measurements using samples of known length. Unrefined versions of this technique typically give a measurement resolution of approximately one-quarter of a wavelength.[23] Thus, it is desirable to use as high a frequency as possible for the measurement.

The measurement of the burning rate of a solid propellant uses the same concept. Thickness is measured repeatedly during the experiment. The derivative with respect to time of these measurements represents the burning rate of the propellant. To make accurate measurements of transient burning rates, however, high precision in the ultrasound measurement is required. For practical reasons, such as acoustic attenuation at high frequencies, ultrasound measurements in propellants are typically made with pulse frequencies on the order of 1 MHz. The speed of sound in a propellant is around 2000 m/s. These figures yield a wavelength of 2 mm, which, using the technique outlined earlier, will result in a precision of $\pm 500\ \mu$m in each distance measurement. Solid propellant may have a burning rate of 5 mm/s or lower. Thus, precise measurement of burning rate using this technique would require very high numbers of measurements per second and averaging over relatively long timescales.

Measurements are further complicated because propellant is not an acoustically simple solid. Modern propellants, such as those used in this study, are nonlinear viscoelastic particulate composites. A burning propellant has a rough surface, which may or may not be covered with melting binder and/or aluminum. The chamber pressure compresses the propellant. The large temperature gradient in the thermal layer at the surface affects the propellant density, speed of sound, and acoustic impedance. We will deal with each of these phenomena in the following paragraphs.

To improve the accuracy of the ultrasound method over the one-quarter wavelength quoted earlier, one must use more sophisticated techniques to detect the echo. Accuracy can be improved by several orders of magnitude by measuring the phase of the reflected waveform. For instance, Royer and Casula[24] describe a technique where displacements of a moving surface are measured with an accuracy of 0.1 nm using only a 50-μm acoustic wavelength, a sensitivity of 2×10^{-6} times the wavelength. Similar results were obtained using ultrasound interferometry.[25]

Some techniques for measuring propellant burning rates have used methods that only approximately measure the phase of the ultrasound echo. For instance, one could detect certain peaks, troughs, or zero crossings (e.g., Refs. 5 and 6) of the waveform. All of these methods are based on the assumption that the detected feature of the received echoes is essentially invariant. If this assumption is violated, these estimates are likely to be biased.[26] In some cases, the bias error can be much greater than the standard deviation of the measurement. Thus, care should be exercised in selecting a technique.

Figure 1 shows a schematic of the propellant geometry and ultrasound system. The transducer (Panametrics V614-SB 1-MHz unfocused piezoelectric transducer) is separated from the propellant by a buffer rod (Panametrics VHTD-4-1 delay line), which protects the transducer from the hot chamber gases. Both the interface between the buffer rod and the propellant and the propellant surface will return echoes. A typical echo trace is shown in Fig. 2. As the propellant burns, its surface echo will move to the left on the chart. The propellant thickness is calculated by measuring the movement

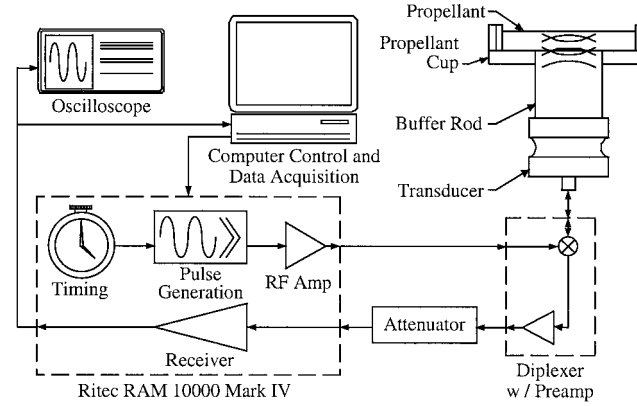

Fig. 1 Schematic of propellant geometry and ultrasound system.

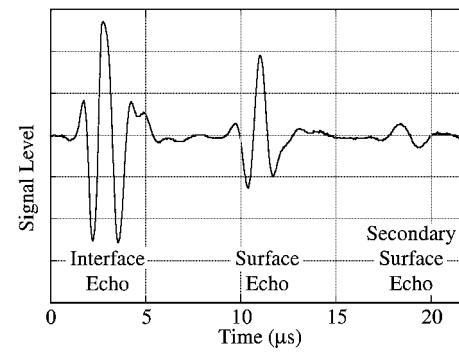

Fig. 2 Typical ultrasound echo record.

of the surface echo relative to the interface echo. Because the interface echo is used as a reference, effects such as the compression of the buffer rod are accounted for.

A Ritec RAM-10000 ultrasound system is used both to pulse the transducer, at a pulse repetition rate of up to 10 kHz, and to receive the resulting echoes. The echoes are recorded digitally at 25 MHz using a Gage Systems CS8500 high-speed data acquisition board. The data are postprocessed using MATLAB® and various digital signal processing techniques to determine the relative movements of the surface and interface echoes, thus determining thickness. The details of these signal processing techniques will be covered after a brief discussion of acoustic wave propagation in propellants.

Propellant Acoustics

Ultrasound wave propagation in a viscoelastic material is governed by the wave equation[27]

$$M(\omega)\frac{\partial^2 u}{\partial x^2} = \rho\frac{\partial^2 u}{\partial t^2} \tag{2}$$

$M(\omega)$ is the bulk longitudinal modulus of the propellant. It is the appropriate modulus for one-dimensional propagation in an infinite medium,[28] which our geometry approximates. $M(\omega)$ is complex and a function of frequency for viscoelastic materials and is related to the bulk modulus $K(\omega)$ and the shear modulus $G(\omega)$ through the relation

$$M(\omega) = K(\omega) + \tfrac{4}{3}G(\omega) \tag{3}$$

The bulk modulus and shear modulus are related to each other through Poisson's ratio:

$$K(\omega) = -\frac{2}{3}\left[\frac{\nu(\omega) - 1}{2\nu(\omega) - 1}\right]G(\omega) \tag{4}$$

Poisson's ratio for propellants is typically very close to 0.5 (see Ref. 29). Thus, $K(\omega)$ is much larger than $G(\omega)$, and Eq. (3) is dominated by the bulk longitudinal modulus.

We will assume a solution to Eq. (2) of the form

$$u(x, t) = \boldsymbol{A}(\omega)\exp[-\alpha(\omega)x]\exp\{i\omega[t - x/c(\omega)]\} \tag{5}$$

Substituting Eq. (5) into Eq. (2) and solving, we find that

$$c(\omega) = \frac{|M(\omega)|}{\sqrt{\rho}}\frac{\sqrt{2|M(\omega)| - 2M_r(\omega)}}{M_i(\omega)} \tag{6}$$

$$\alpha(\omega) = \frac{\omega\sqrt{\rho}}{2|M(\omega)|}\sqrt{2\,|M(\omega)| - 2M_r(\omega)} \tag{7}$$

Because of the dependence of M on frequency, both speed of sound and attenuation are also dependent on frequency; in other words, viscoelastic material is dispersive. Note also that both c and α depend on the square root of density. The preceding equations represent the propagation of a continuous wave at a single frequency. In our application, we send out a pulse, which can be represented as a superposition of many continuous waves:

$$\hat{u}(x, t) = \int_{-\infty}^{\infty} u(x, t)\,\mathrm{d}\omega$$

$$= \int_{-\infty}^{\infty} \boldsymbol{A}(\omega)\exp[-\alpha(\omega)x]\exp\left\{i\omega\left[t - \frac{x}{c(\omega)}\right]\right\}\mathrm{d}\omega \tag{8}$$

Although the harmonic components of the pulse travel at different phase speeds, the pulse itself travels at its own velocity, the group velocity; this is the velocity at which information in the system propagates.[30] Formally, the group velocity is given in terms of the wave number $k(\omega) = \omega/c$:

$$\boldsymbol{C} = \frac{\partial\omega}{\partial k} \tag{9}$$

Throughout the remainder of this paper, we will treat the distinction between phase velocity and group velocity somewhat loosely. In every case where we go from the measured time delay to a distance, the proper value to use for the speed of sound is the group velocity.

Our discussion so far has focused on the viscoelastic nature of the propellant. Another propellant component that greatly affects both dispersion and attenuation characteristics is the oxidizer particles. As already mentioned, the combination of polymer binder and crystalline oxidizer particles forms a random particulate composite. A fair amount of research, both experimental (e.g., Ref. 31) and theoretical (e.g., Refs. 32 and 33), has been conducted regarding wave propagation in these types of materials. In general, the results show that the acoustic attenuation will peak at a critical normalized frequency (the product of the wave number k and the particle radius $d/2$) of order one. This is to be expected because the particles will scatter very efficiently when the wavelength is approximately equal to their characteristic dimension. The region where normalized frequency is less than the critical value is known as the acoustical branch, whereas the region where normalized frequency is greater than the critical value is known as the optical branch. In the acoustical branch, particles move in phase with the surrounding matrix, whereas particles move out of phase with the matrix in the optical branch. There is typically a large jump in the propagation speed when moving between branches.

Attenuation in our propellant, which has 200-μm-diam oxidizer particles, limits us to a frequency of around 1 MHz. The normalized frequency is approximately 0.3, placing our experiment in the acoustical branch. For the fine oxidizer (2 μm diam) and binder matrix, the normalized frequency is a much smaller 0.003.

Both the viscoelastic binder and the particulate oxidizer contribute to frequency-dependent attenuation in the propellant. This phenomenon causes a pulse that has traveled through a thick piece of propellant to have less high-frequency content than one that has traveled through a thin piece. The resulting shift in the peak frequency can contribute substantial error in Doppler shift applications (see Ref. 34). The shape of the waveform is also affected, which can cause error in time-of-flight measurements. The measurement technique must, therefore, be chosen with care to minimize this type of error.

Signal Detection

Application of ultrasound echo location to measure displacement centers around estimating the time delay between two echoes. Time delay estimation, which is an active area of signal processing research and development,[35] is typically done using a cross correlation formally defined for a finite sequence of length T as

$$R_{xy}(\tau) = \frac{1}{T}\int_0^T x(t)y(t + \tau)\,\mathrm{d}t \tag{10}$$

The value of τ at which the cross correlation has a maximum is the time delay between the two signals.[36] Cross correlation is an unbiased technique for estimating time of flight in nondispersive systems[26] and is relatively insensitive to changes in spectral information due to attenuation.

The envelope of Eq. (10) is calculated by taking the quadratic sum of the cross correlation and its Hilbert transform, that is,

$$\boldsymbol{A}_{xy}(\tau) = \left[R_{xy}^2(\tau) + \tilde{R}_{xy}^2(\tau)\right]^{\frac{1}{2}} \tag{11}$$

The maximum of the envelope function $\boldsymbol{A}_{xy}(\tau)$ is a better estimate of the time delay than the maximum of the cross correlation $R_{xy}(\tau)$, when testing a dispersive material. When no dispersion is present, the two maxima will coincide. When dispersion is present, using the cross-correlation maximum will introduce an error into the measurement of up to $\pm\pi/\omega_0$ (Ref. 37) (± 3.14 μs using a 1-MHz transducer). The drawback to using the envelope function is that its peak is very broad, and, thus, its placement is harder to detect accurately. Therefore, we use the cross correlation rather than the envelope function in our measurements. Because we are cross

correlating two echoes, rather than a transmitted wave and an echo, errors from dispersion are much less than the $\pm\pi/\omega_0$ quoted earlier.

Our ultrasound signals are sampled at 25 MHz, giving a time-lag resolution of 40 ns for the cross correlation without interpolation. This amounts to a spatial resolution of about 80 μm for the thickness measurement. To improve this number, the maximum of a parabola, fitted to the points in the neighborhood of the peak, is used to estimate the time delay. Unfortunately, this technique is not free from bias, with both the variance and the bias depending on signal-to-noise ratio, signal and noise bandwidth, and the location of the delay between samples.[38,39]

As the propellant thickness approaches the acoustic wavelength, the echoes begin to overlap. The described techniques rely on the primary surface echo being separable from the interface echo and any secondary surface echoes. This problem is quite common in nondestructive testing applications.[25,40] Techniques developed to deal with this problem generally use the cepstrum of the signal associated with a deconvolution.[40–42] (The complex cepstrum is defined as the inverse Fourier transform of the logarithm of the complex spectrum of a signal. See Chapter 12 of Ref. 43 for more details.) Cepstrum techniques have not, however, proven to be useful in our application. We have improved the detection of the primary surface echo by subtracting out the interface echo before doing the cross correlation.

Figure 3 shows traces from two echoes recorded 0.5 s apart during a steady-state experiment. The first pulse seen in the traces is the echo from the interface between the buffer rod and the bottom of the propellant. The second pulse, which is highlighted in Fig. 3, is the primary echo from the propellant surface: It is this echo that we are interested in. One can also see a third pulse in the second trace, which is a secondary echo from the surface. This echo occurs because some of the energy from the primary echo did not pass through the interface, but rather was reflected back into the propellant, and made a second round-trip.

The primary surface echoes from the two traces are separated out and cross correlated with each other. Figure 4 shows the cross correlation and its envelope. The time lag between the echoes is the maximum of the envelope function and is labeled τ in Fig. 4. Figure 4 shows that there is little difference between the peak of the cross correlation and the peak of the envelope function. Figure 5 shows the two primary surface echoes superimposed on each other. One of the echoes has been shifted by the measured time delay.

Static tests with nonburning propellant samples indicate that the precision error in a single time delay estimate using the techniques already outlined, with a center acoustic frequency of 1 MHz and a sample rate of 25 MHz, is approximately ± 4 ns, which amounts to a distance resolution of ± 8 μm. This number is an order of magnitude better than the ± 80 μm quoted earlier in this paper. The improvement is due to the use of a fitted parabola to find the peak. The resolution can undoubtedly be improved further by increasing the sample rate or using more sophisticated digital signal processing techniques.[26,44–46] Note that this number is an indication of the signal-to-noiseratio of the measurement and not the measurement's ultimate accuracy. Precision error affects the practicality of the measurement. The lower the precision, the more measurements you must take to average out noise. Accuracy, on the other hand, depends on bias errors in the measurement.

Figure 6 shows data from a 50-Hz experiment. Propellant thickness is shown in Fig. 6a. Figure 6b shows burning rate, which

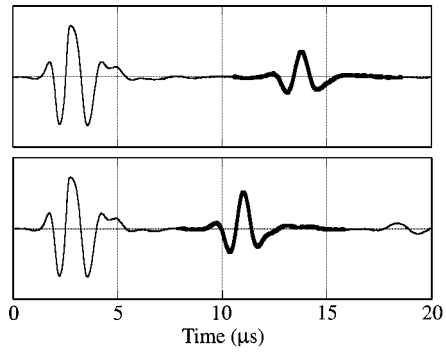

Fig. 3 Ultrasound echoes recorded 0.5 s apart during a steady-state experiment; primary surface echoes are highlighted.

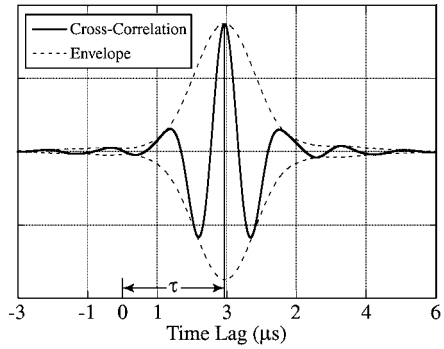

Fig. 4 Cross correlation and the cross-correlation envelope function of the two primary surface echoes shown in Fig. 3.

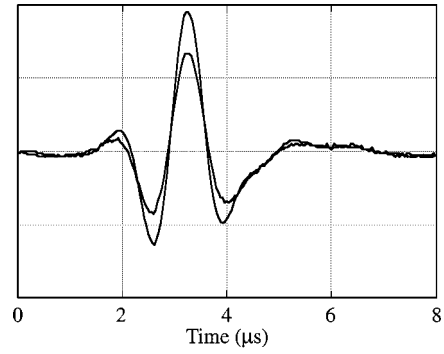

Fig. 5 Echoes shown in Fig. 3, shifted by the measured time delay.

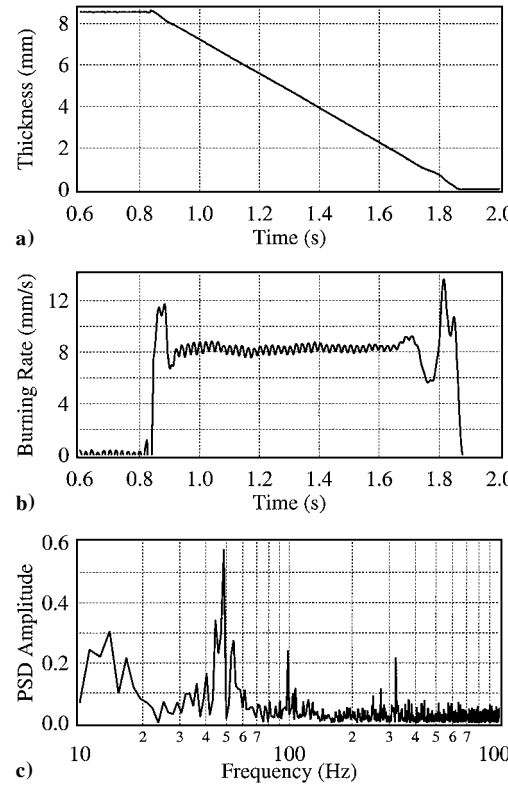

Fig. 6 Propellant thickness, burning rate, and the power spectral density of the unsteady component of the propellant thickness.

was calculated using a differentiation filter with a cutoff frequency at 50 Hz. The oscillations are clearly visible in the burning rate. Figure 6c shows the power spectral density function, which was calculated directly from a fast Fourier transform without any averaging to improve signal-to-noise ratio, of the unsteady part of the thickness measurement. The 50-Hz oscillation is clearly visible in Fig. 6c as well. When moving to higher frequencies, it becomes much harder to pick out the oscillation in the burning-rate trace (which is calculated using a differentiation filter with a higher cutoff frequency), but it is still easy to see it in the power spectral density plot.

Response Function Calculation

Calculation of the response function from the measured data requires estimation of the spectral magnitude and phase of the burning-rate signal and the pressure signal at the frequency of the test. An estimate of the response function is obtained by taking the Fourier transform of the burning rate and dividing by the Fourier transform of the pressure, that is,

$$\boldsymbol{R} = (\bar{\dot{r}}/\bar{p})(G_{\dot{r}}/G_p) \tag{12}$$

Because burning rate is the derivative of web thickness, an equivalent equation is

$$\boldsymbol{R} = i\omega(\bar{\dot{r}}/\bar{p})(G_x/G_p) \tag{13}$$

Pressure Correction

When the combustion chamber is pressurized, the propellant will be compressed. This compression will cause a change in the propellant thickness, as well as a change in the speed of sound. If these errors are not corrected, they will corrupt the burning-rate measurement.

If viscoelastic effects are ignored at slow timescales, the pressure effects are relatively easy to correct. For steady-state burning-rate measurements, pressure effects can be corrected by using an effective speed of sound c_{eff}, which includes both the compression of the propellant and the change in the actual speed of sound. The effective speed of sound is measured by pressurizing the chamber with a piece of nonburning propellant in it and recording the change in round-trip-time during the test, that is,

$$c_{\text{eff}}(p)/c_r = \Delta t_r/\Delta t(p) \tag{14}$$

Then, this effective speed of sound can be used to calculate the web thickness during the actual tests.

In the oscillatory tests, experimental uncertainty in the measurement of the phase of the pressure and web thickness can introduce large errors into the pressure correction at high frequencies. Thus, the corrections for the steady-state and oscillatory parts of the pressure are treated separately. The steady-state correction can be performed as already outlined; oscillatory correction is developed next.

Taking the derivative of Eq. (1), expanding time-dependent terms into steady and unsteady components, and subtracting out the steady-state ones, we have

$$\frac{\dot{r}'}{\bar{\dot{r}}} = \frac{c'_{\text{eff}}}{\bar{c}_{\text{eff}}} + \frac{\dot{\delta}'}{\bar{\dot{\delta}}} + \frac{\delta}{\bar{c}_{\text{eff}}\bar{\dot{\delta}}}\frac{\mathrm{d}c_{\text{eff}}}{\mathrm{d}t} + \frac{c'_{\text{eff}}}{\bar{c}_{\text{eff}}}\frac{\dot{\delta}'}{\bar{\dot{\delta}}} \tag{15}$$

where Δt has been rewritten as δ. Note that $\delta'/\bar{\dot{\delta}}$ is what we are actually measuring. The last term in Eq. (15) is higher order and is neglected.

We write the change in the effective speed of sound in terms of the pressure, that is, $c'_{\text{eff}}/\bar{c}_{\text{eff}} = (\mathrm{d}c_{\text{eff}}/\mathrm{d}p)(p'/\bar{p})$. Note that $\mathrm{d}c_{\text{eff}}/\mathrm{d}p$ can be complex, allowing for viscoelastic effects. After dividing through by the unsteady pressure, we can write the response function as a measurement plus a correction:

$$\boldsymbol{R}_{\dot{r},p} \equiv \frac{\dot{r}'/\bar{\dot{r}}}{p'/\bar{p}} = \underbrace{i\omega\frac{\delta'/\bar{\dot{\delta}}}{p'/\bar{p}}}_{\text{measurement}} + \underbrace{\left(1 + i\omega\frac{\delta}{\bar{\dot{\delta}}}\right)\frac{\bar{p}}{\bar{c}_{\text{eff}}}\frac{\mathrm{d}c_{\text{eff}}}{\mathrm{d}p}}_{\text{correction}} \tag{16}$$

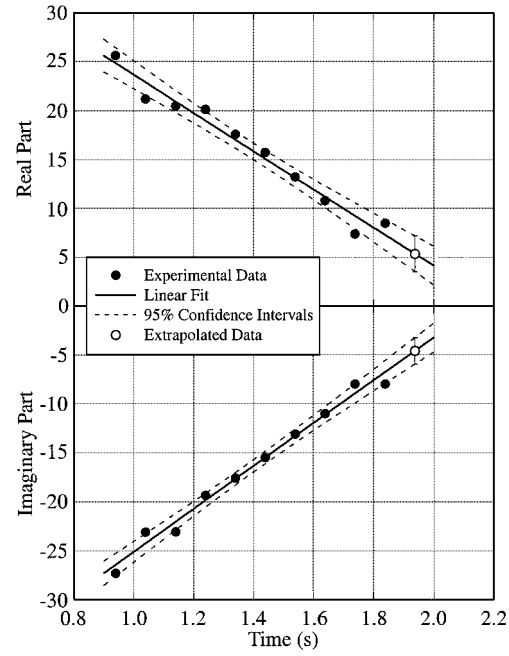

Fig. 7 Real and imaginary part of the measured response function from a 200-Hz experiment with the UTP propellant 8. Linear fit and 95% confidence intervals are extrapolated to the burnout time of the propellant to estimate the actual pressure-corrected response function.

The second term of the correction factor dominates this equation for most of the experiment. This term includes the quantity δ, which is approximately a linear function of time. Thus, when we look at the time-resolved response function for an experiment, we would expect to see a linear decrease with time. The real and imaginary parts of the measured response function can then be fit to straight lines. Then the fit can be extrapolated out to when the propellant burns out, and the term in Eq. (16) proportional to web thickness is zero.

Data from a 200-Hz experiment are shown in Fig. 7. The time-resolved real and imaginary parts of the response function are shown. The linear fit for each is extrapolated out to the burnout time of the propellant. Because the fits are calculated from a group of observations, random error can be estimated from the statistics of those observations. Thus, the linear fits provide not only estimated values of the real and imaginary parts of the response function, but also 95% confidence intervals for those values. The confidence intervals of the response function estimates are also shown in Fig. 7.

Note that this technique does not require the value of $(\bar{p}/\bar{c}_{\text{eff}})\,\mathrm{d}c_{\text{eff}}/\mathrm{d}p$ to be known a priori. This physical property is determined from the analysis: It is proportional to the slope of the linear fit. This independence of the propellant properties is advantageous because viscoelastic properties of propellants are notorious for depending on such difficult-to-control variables as prior loading history. Note that it is also unnecessary to determine the value of c_{eff} to determine the response function, although this value is still necessary for accurate determination of the mean burning rate.

The magnitude and the phase of the response function are calculated from the real and imaginary parts. Estimates of the uncertainties of these values are calculated from the confidence intervals of the real and imaginary parts using the following formulas:

$$\delta|\boldsymbol{R}| = \frac{\sqrt{\boldsymbol{R}_r^2(\delta\boldsymbol{R}_r)^2 + \boldsymbol{R}_i^2(\delta\boldsymbol{R}_i)^2}}{|\boldsymbol{R}|} \tag{17}$$

$$\delta \arg \boldsymbol{R} = \frac{\sqrt{\boldsymbol{R}_r^2(\delta\boldsymbol{R}_i)^2 + \boldsymbol{R}_i^2(\delta\boldsymbol{R}_r)^2}}{|\boldsymbol{R}|^2} \tag{18}$$

Thermal Boundary Layer

The speed of sound is highly dependent on the temperature of the propellant. Because of this, the thermal boundary layer at the propellant's surface, which changes during a burning-rate transient, can cause systematic errors in the measurement.[11] Measuring the speed of sound in a propellant at high temperatures is not practical. However, making several assumptions about the behavior of the propellant properties, we can use properties at lower temperatures to estimate the properties a higher temperatures. The approximate thermal profile can be calculated assuming one-dimensional heat conduction in a homogeneous solid with constant properties and a moving boundary. For the steady-state case,

$$\frac{\bar{T}(x/\xi) - T_0}{\bar{T}_s - T_0} = \exp\left(\frac{x}{\xi}\right) \tag{19}$$

where $\xi = \alpha/\bar{\dot{r}}$ is the characteristic thermal-layer thickness. For the transient case, the governing equation is nonlinear as a result of the moving boundary. Thus, no analytical solution is available. However, we can solve the linearized version to find an expression for thermal profile relevant to our oscillatory experiments:

$$\frac{T'(x/\xi) - T_0}{\bar{T}_s - T_0} = \left\{\frac{1}{\lambda}\exp\left(\frac{\lambda x}{\xi}\right)\boldsymbol{R}_{f_s,p} + \frac{1}{\lambda^2 - \lambda} \times \left[\frac{1}{\lambda}\exp\left(\frac{\lambda x}{\xi}\right) - \exp\left(\frac{x}{\xi}\right)\right]\boldsymbol{R}_{\dot{r},p}\right\}\frac{p' - \bar{p}}{\bar{p}}\exp(i\omega t) \tag{20}$$

The parameter λ is written in terms of the nondimensional frequency, $\Omega = \omega\alpha/\bar{\dot{r}}^2$:

$$\lambda = \left(1 + \sqrt{1 + 4i\Omega}\right)/2 \tag{21}$$

The $\boldsymbol{R}$ represents frequency-response functions for burning rate and heat flux, given here in terms of the "flame model" parameter set from a quasi-steady gas-phase and solid-phase reaction layer, homogeneous, one-dimensional solid (QSHOD)[47–49]:

$$\boldsymbol{R}_{\dot{r},p} \equiv \frac{(\dot{r} - \bar{\dot{r}})/\bar{\dot{r}}}{(p - \bar{p})/\bar{p}} = \frac{nAB + n_s(\lambda - 1)}{\lambda + A/\lambda - (1 + A) + AB} \tag{22}$$

$$\boldsymbol{R}_{f_s,p} \equiv \frac{(f_s - \bar{f}_s)/\bar{f}_s}{(p - \bar{p})/\bar{p}} = -\frac{1}{\lambda}\frac{nAB + n_s(\lambda^2 - 1) + B\lambda^2(n - n_s)}{\lambda + A/\lambda - (1 + A) + AB} \tag{23}$$

These expressions are derived in the Appendix. The burning-rate response $\boldsymbol{R}_{\dot{r},p}$ is measured during our experiment; the heat-flux response $\boldsymbol{R}_{f_s,p}$ is not. We would like to put $\boldsymbol{R}_{f_s,p}$ in terms of $\boldsymbol{R}_{\dot{r},p}$, if possible. If we assume that $n_s \approx 0$, we find that

$$\boldsymbol{R}_{\dot{r},p} = \frac{nAB}{\lambda + A/\lambda - (1 + A) + AB} \tag{24}$$

$$\boldsymbol{R}_{f_s,p} = -\frac{1}{\lambda}\frac{nAB(1 + \lambda^2/A)}{\lambda + A/\lambda - (1 + A) + AB} = -\left(\frac{1}{\lambda} + \frac{\lambda}{A}\right)\boldsymbol{R}_{\dot{r},p} \tag{25}$$

This allows us to calculate the thermal profile in the propellant using the value of the burning-rate-response function and only one of the QSHOD parameters, A, rather than three. The parameter n_s, which represents the pressure dependence of burning rate at constant surface temperature, has traditionally been considered to be very small. However, theoretical and experimental evidence supporting this presumption is sketchy at best. In light of the approximation we have already made that the QSHOD model a suitable representation of a composite propellant, we feel that the assumption that $n_s \approx 0$ is reasonable, especially because this analysis is used only to estimate error.

Our next task is to estimate the effect of temperature on the speed of sound in the propellant. For this analysis, we will assume that the propellant is a thermorheologically simple material, although studies have shown that this is not necessarily true.[50] When a material is thermorheologically simple, modulus vs frequency curves at different temperatures can be collapsed into a single, master curve, that is, $M(\omega, T) = M(\omega a_T)$, where a_T is the temperature shift factor. This phenomenon is known as time–temperature equivalence. Empirically, a_T usually can be fit to the following equation:

$$\log(a_T) = -\frac{C_1(T - T_r)}{C_2 + (T - T_r)} \tag{26}$$

This equation is known as the Williams–Landel–Ferry (WLF) equation (see Refs. 28 and 51). It has been used to correlate experimental data from a wide range of viscoelastic materials,[28,51–53] including ammonium perchlorate (AP)–hydroxyl-terminated polybutadiene (HTPB) propellants.[29,54,55] From Eq. (3), we see the dependence of the propagation modulus on the bulk and shear moduli. Measurements of the shear modulus $G(\omega)$ are available in Ref. 29, but measurements of the bulk modulus $K(\omega)$ are not. We will, thus, assume that the bulk modulus behaves similarly to the shear modulus:

$$M(\omega a_T)/M_r \approx G(\omega a_T)/G_r \tag{27}$$

The propellant density will change with temperature, affecting the speed of sound and the physical length of the propellant. Because these effects are small and tend to cancel out (lower density increases the speed of sound, but the propellant also becomes longer), we will ignore them in this analysis. Thus, to estimate the speed of sound as a function of temperature, we first use Eq. (26) with $C_1 = 5.1$, $C_2 = 163$ K, and $T_r = 296$ K (Ref. 29), to calculate the temperature shift factor a_T. Then the bulk longitudinal modulus is estimated using Eq. (27) and the data for shear modulus at 2% dynamic strain in Ref. 29. Finally, Eq. (6) is used to calculate the speed of sound. Speed of sound vs temperature is shown in Fig. 8.

The error in the distance measurement caused by the steady-state thermal boundary layer can be calculated by integrating the speed of sound profile in the propellant:

$$\delta x = \xi\left\{\int_0^{h/\xi} \frac{1}{c[T(x/\xi)]/c_r}\,\mathrm{d}\left(\frac{x}{\xi}\right) - \frac{h}{\xi}\right\} \tag{28}$$

We see that this error is proportional to the thermal boundary-layer thickness. Thus, it is inversely proportional to the burning rate. This is true regardless of the actual variation of the speed of sound with temperature. Using the steady-state thermal profile [Eq. (19)] and assuming an initial temperature of 300 K and a surface temperature of 800 K, we find that the error in the distance measurement is 2.72 times the thickness of the thermal layer.

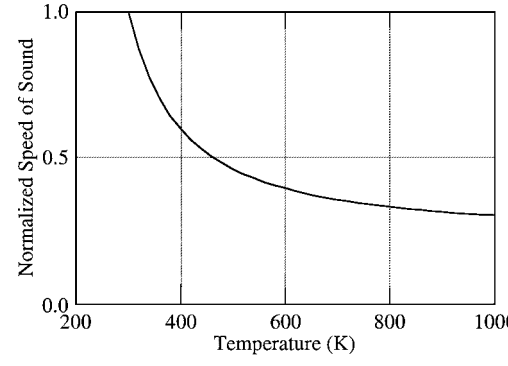

Fig. 8 Estimated speed of sound, normalized to its value at 300 K, vs temperature for an AP–HTPB propellant.

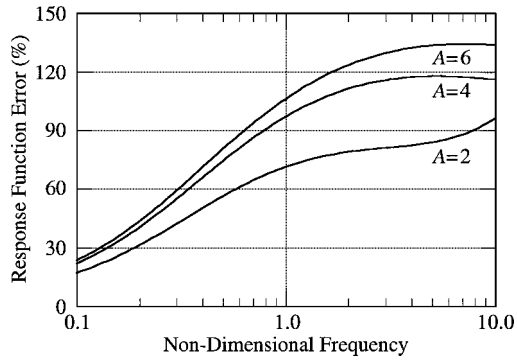

Fig. 9 Burning-rate response function measurement error due to the thermal layer in the propellant (note that error depends on nondimensional frequency, rather than absolute frequency).

Thus, for a monotonic experiments, where the timescale of the transient is larger than the thermal timescale of the propellant, the error in the burning rate is

$$\delta\dot{r} = \frac{2.72(\xi_f - \xi_i)}{\text{transient timescale}} \tag{29}$$

To estimate the error in a response function measurement, we again use Eq. (28) with the thermal profile given by Eq. (20). We calculate the amplitude of δx as a function of frequency. The burning-rate error is then determined by taking a derivative with respect to time. Response function measurement error using a surface temperature of 800 K and an initial temperature of 300 K is shown in Fig. 9 as a function of frequency and the parameter A. The values of A that are shown are consistent with the burning-rate and surface temperature measurements made by Mench et al.[56] Note that the error is a function of nondimensional frequency, $\Omega = 2\pi f\alpha/\dot{r}^2$. Thus, error is determined by a combination of frequency and burning rate, rather than just frequency. These results are consistent with those of other researchers.[12]

Surface Roughness

The veracity of the ultrasound measurement for transient burning rates of composite propellants is sometimes questioned (e.g., Ref. 57) because of the requirement that the technique measure changes in the length of the propellant that are smaller than the surface roughness of the propellant. This question arises partly because of the ambiguity in specifying the length of something that has rough ends. In regards to our experiment, this is a moot point because we are interested in changes in the length, not absolute length. In principle, there is no uncertainty in specifying the change in position of any surface, no matter how rough, as long as the structure of the surface does not change.

Problems arise because the surface structure of the propellant does change during transients, at least in some cases. There are currently no models that can predict the evolution of surface structure during nonsteady burning. The best we can do is make some general statements about the nature of surface roughness effects on acoustic wave reflection.

The interaction of an acoustic wave with a rough surface will be highly dependent on the ratio of the acoustic wavelength to the roughness length scale. Our experiment operates in a regime where the wavelength of the ultrasound (2 mm) is much greater than the scale of the surface roughness (assumed to be on the order of the oxidizer particle size, 200 μm). The rough surface thus appears to be smooth to the acoustic wave and will not affect the measurement very much. One research group has used computer simulations to look at roughness effects on propellant burning rate measurements.[58] Their results primarily concern cases where the scale of roughness on the propellant surface is much larger than 200 μm. Also, the results are presented in terms of the effect on the zero crossing of the ultrasound signal and are, thus, not directly applicable to our experiments because we use cross correlation.

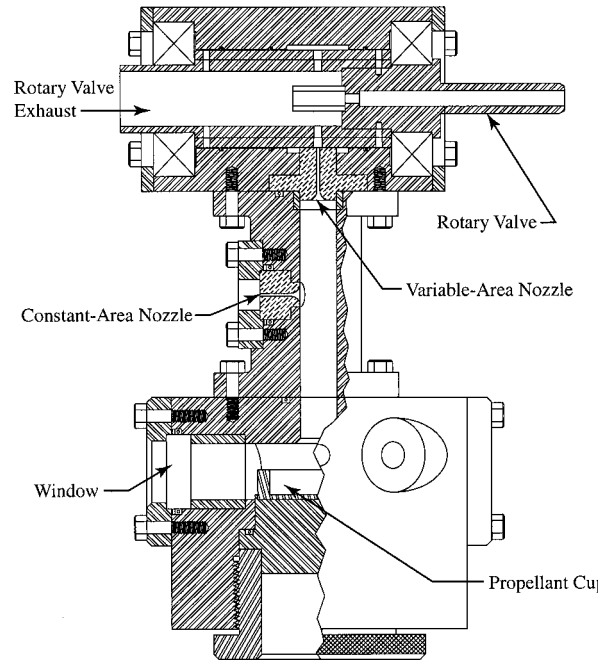

Fig. 10 Schematic of oscillatory burner.

Another point is that our experiment uses unfocused transducers. The measurement is made over a surface approximately 2.5 cm (1 in.) in diameter. This helps make the technique insensitive to local changes in the topology of the propellant surface because the measurement is essentially averaged over that area.

Experimental Apparatus

Our oscillatory burner (Fig. 10) is a rotating valve design based on that developed at United Technologies Chemical Systems Division (CSD).[59,60] The main difference is that our configuration is an end burner, whereas CSD uses a cylindrical grain. Our propellant sample is approximately 32 × 32 mm (1.25 × 1.25 in.). The ultrasound transducer sits beneath the propellant sample. The motor is designed to operate at pressures up to 204 atm (3000 psi). Control over the average chamber pressure and the amplitude of the pressure oscillations is accomplished by varying the sizes of the constant-area and variable-area nozzles. Oscillation amplitude can also be increased by inserting a sleeve into the chamber, reducing its internal volume. Maximum oscillation frequency with the current motor and pulley setup is approximately 600 Hz. More details of the experimental setup are available in Refs. 61 and 62.

Summary of Data Reduction Procedure

The frequency of a test is measured by looking at the power spectrum of the pressure record from that test. The error in the reported frequency is ±0.04 Hz.

The response function is determined from the pressure and propellant thickness data using the following procedure:

1) The slowly varying steady-state part of the pressure and thickness are determined as functions of time by applying a low-pass digital filter with a cutoff frequency of 5 Hz.

2) The mean pressure is calculated from the filtered data.

3) The mean burning rate is calculated from the slope of a linear regression of the web thickness data. This burning rate is generally not corrected for mean pressure effects on the effective speed of sound c_{eff} because these effects do not change the measured value of the response function.

4) The unsteady part of pressure and thickness are obtained by subtracting the steady-state part from the original data.

5) A discrete Fourier transform is applied to the unsteady data at the frequency of interest. A moving window, 0.1 s in width, is used to calculate the time-resolved spectral power.

6) The time-resolved response function is calculated using Eq. (13).

7) The values of the real and imaginary part of the response function are calculated from the data using the linear curve-fitting technique described earlier.

When more than one test has been run under a given set of conditions, the data points are averaged to get a better estimate of the response function at those conditions. The individual experiments are weighted inversely to their error, so that the good experiments have more weight than the bad:

$$\langle \boldsymbol{R} \rangle = \frac{\Sigma(\boldsymbol{R}/\delta\boldsymbol{R})}{\Sigma(1/\delta\boldsymbol{R})} \tag{30}$$

The error in the weighted average is estimated by taking a weighted average of the errors of the individual experiments and dividing by the square root of the number of experiments. This estimate turns out to be the harmonic mean of the individual errors:

$$\langle \delta\boldsymbol{R} \rangle = \frac{\sqrt{N}}{\Sigma(1/\delta\boldsymbol{R})} \tag{31}$$

Results and Discussion

Three propellants manufactured by Thiokol Corporation and one propellant manufactured by United Technologies CSD were tested. The formulations of these propellants are shown in Table 1. The response function data are plotted in terms of nondimensional frequency, $\Omega = 2\pi f \alpha / \bar{r}^2$, where f is dimensional frequency in hertz and α is the thermal diffusivity of the propellant. We used $\alpha = 1.2 \times 10^{-3}$ cm^2/s and $\alpha = 1.5 \times 10^{-3}$ cm^2/s for the nonaluminized and aluminized propellants, respectively.[63] The actual frequencies of the tests shown ranged from 20 to 300 Hz. The unsteady pressure amplitude was typically between 1 and 5% of the mean pressure, although the amplitude was between 6 and 8% for a few of the tests reported here. Filled symbols in Figs. 12–15 denote individual experiments, whereas open symbols denote averages. The data shown in Figs. 11–15 is tabulated in Ref. 62.

Figure 11 shows the mean burning rates from all of the oscillatory tests of Thiokol propellant 10, the nonaluminized propellant. The error bars on the plot represent the statistical uncertainties in obtaining mean values from oscillating signals. These data show good agreement with strand-burner data from Thiokol. Measuring the steady-state burning rate of the propellant gives us an important cross check to ensure that the experiment was operating properly.

Table 1 Propellant formulations tested

Designation	AP	Aluminum	Binder	Curative
Thiokol 10	55% 200μm/33% 2μm	0%	HTPB	DDI
Thiokol 1a	39% 200μm/31% 2μm	15% 100μm	HTPB	DDI
Thiokol 2	44% 200μm/26% 2μm	15% 100μm	HTPB	IPDI
UTP 8	41% 200μm/28% 2μm	19% 25μm	HTPB	DDI

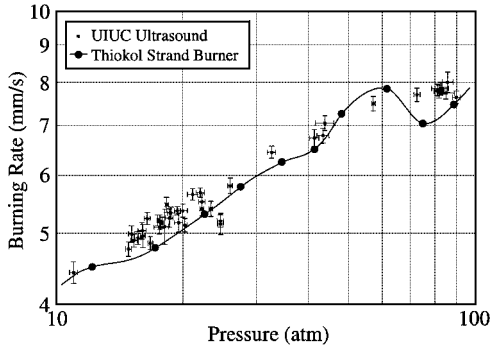

Fig. 11 Measurements of mean burning rate of Thiokol propellant 10 during the oscillatory experiments. Data show good agreement with measurements of the steady-state burning rate made by Thiokol using a strand burner.

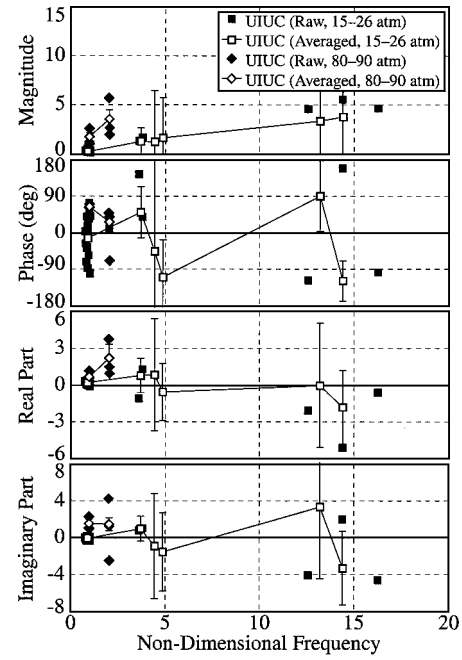

Fig. 12 Response function measurements for Thiokol propellant 10.

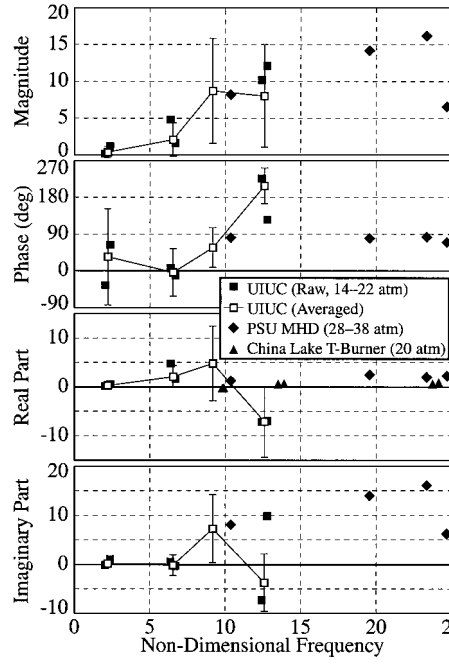

Fig. 13 Response function measurements for Thiokol propellant 1a.

Figure 12 shows response function magnitude for Thiokol propellant 10 in two pressure ranges: 15–26 atm and 80–90 atm. The tests show reasonable repeatability, even at high frequency. The results also demonstrate that the measurement technique can distinguish differences in propellant response function under different operating conditions. The response is noticeably higher at the higher pressure.

Figure 13 shows the response function for Thiokol propellant 1a. These data are compared with measurements made using a magnetic flowmeter[20,64] at Pennsylvania State University. The magnetic flowmeter directly measures the propellants's acoustic admittance (nondimensional acoustic pressure divided by nondimensional acoustic velocity) as a function of distance above the propellant's surface. The acoustic velocity is determined by imposing a strong magnetic field across the combustion products, which are electrically conductive, and measuring the electric potential. Acoustic

pressure is measured by a piezoelectric pressure transducer located the same distance above the propellant as the velocity measurement. A one-dimensional linear acoustic analysis of the combustion chamber flow is used to calculate the acoustic admittance at the surface of the propellant from the measurements made above the propellant surface. Pressure-coupled burning-rate responses can be calculated from the acoustic admittance. The response function measured with our ultrasound technique agree with the measurements made with the magnetic flowmeter.

The data for the real part of the response shown in Fig. 13 are also compared to measurements made with a T-burner[21] at the Naval Air Warfare Center in China Lake, California. The results are not inconsistent with each other. The ultrasound data show a sharp drop in the real part of the response around a nondimensional frequency of 13. Laser-recoil measurements (currently unpublished) made by Brewster at the University of Illinois show a similar drop in the real part of the response for this particular propellant. More tests need to be conducted to verify this characteristic.

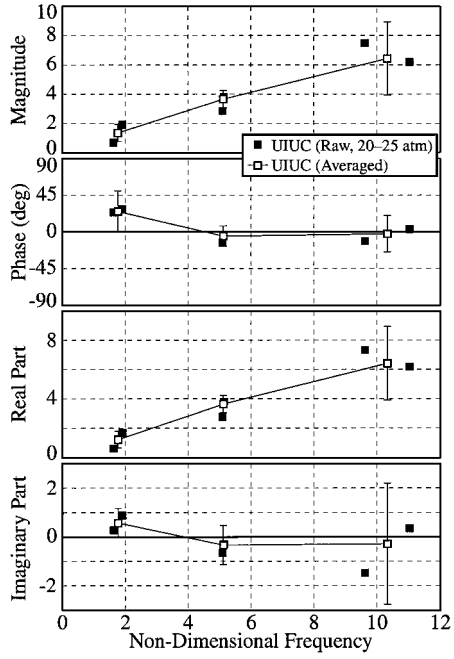

Fig. 14 Response function measurements for Thiokol propellant 2.

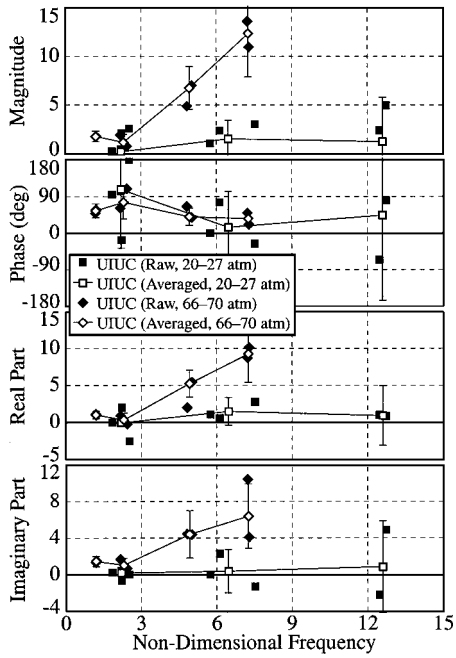

Fig. 15 Response function measurements for United Technologies CSD propellant 8 at two operating pressures.

Data for two other aluminized propellants are shown last. Figure 14 shows response measurements for Thiokol propellant 2, which is a variation of Thiokol propellant 1a with isophorone diisocyanate (IPDI) used in place of dimeryl diisocyanate (DDI) as the curative. The United Technologies propellant (UTP), shown in Fig. 15, was tested at two different pressures: 20 and 70 atm. The results show a marked increase in the measured response function at higher pressure.

The most striking feature of the data is the large error bars shown on some of the measurements. These error bars are an indication of the precision of the measurement, rather than the accuracy. Thus, their size can be reduced as much as is desired by performing more experiments. There are practical limitations, of course. One can reduce the error by a factor of 100 by performing 10,000 experiments, but this is hardly reasonable.

More troubling is the bias error resulting from the thermal boundary layer in the propellant. This error can be very large, more than doubling the measured response function. Thermal boundary-layer error is also the most likely explanation for the rather high values of the real part of the response function (5–10) shown in Figs. 14 and 15. For some applications, such as comparing two propellants with similar material properties, this may not be an issue. Other applications, such as predicting rocket motor stability, will be very sensitive to this error. It appears that actually correcting this error in the measurements would require the use of a material properties model of the propellant.

Conclusions

We have demonstrated the use of ultrasound to measure the pressure-coupled burning-rate response functions of solid-rocket propellants at frequencies up to 300 Hz.

Cross correlation is an accurate, robust method for determining the round-trip time of the ultrasound echo. If the propellant is dispersive at the ultrasound frequencies used, the envelope function of the cross correlation is a more accurate technique than straight cross correlation. We have found, however, that using the envelope function is less robust. Locating the peak in the cross correlation is subjected to bias errors. Thus, care must be exercised when using these techniques.

The burning-rate measurement must be corrected for compression caused by the chamber pressure. When conducting response function measurement experiments, the error term is proportional to the propellant thickness. This linearity of the error term can be exploited to correct the measurement for the effects of compression without a priori determination of the propellant acoustic properties.

The effects of the thermal boundary layer on the measurement were quantified. The measured response function can be twice as much as the actual response function due to this error. Because this error is a bias error, however, response function comparisons among propellants with similar material properties remain valid. Other phenomena that can distort the measurements, such as surface roughness, remain unquantified.

The ultrasound technique has a low signal-to-noise ratio, sometimes resulting in large (>100%) precision errors. These errors are especially evident at higher frequencies, due to the smaller amplitude of the pressure oscillations in our chamber. Although these errors can be reduced by performing multiple experiments, they limit the practicality of the technique. Ultrasound appears to be best suited for making response function measurements at relatively low frequencies (<200 Hz). Because this frequency range is below the minimum frequency at which response function measurements are usually made, opportunities for comparison of ultrasound with these other techiques are limited.

Appendix: Derivation of QSHOD Response Functions

We present a brief derivation of the linear QSHOD frequency-response functions for burning rate and heat flux. The burning rate response function derivation appears quite frequently in the

literature (Refs. 47 and 48, for example). The heat flux response function, however, does not. Thus, we derive both here for completeness. In general, a linear response function represents the solution to a system of linear algebraic equations.[49,65] This system of equations can be represented formally as

$$g_1(T_s, T_i, f_s, \dot{r}, p) = 0, \qquad g_2(T_s, T_i, f_s, \dot{r}, p) = 0$$
$$g_3(T_s, T_i, f_s, \dot{r}, p) = 0 \tag{A1}$$

where T_s is surface temperature, T_i is initial temperature, and f_s is surface heat flux. These equations are the solutions to the partial differential equations that describe the propellant. The three equations loosely correspond to solutions of the condensed-phase heat transfer, condensed-phase reaction layer, and gas-phase equations. We assume that the gas phase is quasi-steady, so that unsteady heat flux can be related to a steady-state heat flux at a different surface temperature, burning rate, and initial temperature using the following equation[49,65]:

$$\frac{\dot{r}'}{\bar{\dot{r}}} - \frac{f_s'}{\bar{f}_s} + \frac{T_s' - T_i'}{\bar{T}_s - \bar{T}_i} + \frac{\dot{r}'}{\bar{\dot{r}}}\left(\frac{T_s' - T_i'}{\bar{T}_s - \bar{T}_i}\right) = 0 \tag{A2}$$

The system of equations shown in Eq. (A1) is linearized and written in matrix form:

$$\begin{pmatrix} 1/B & 0 & 0 & -1 & n \\ 0 & A & 0 & -1 & n_s \\ 0 & -1 & 1/\lambda & -1/\lambda^2 & 0 \\ -1 & 1 & -1 & 1 & 0 \end{pmatrix} \begin{pmatrix} T_i'/(\bar{T}_s - T_i) \\ T_s'/(\bar{T}_s - T_i) \\ f_s'/\bar{f}_s \\ \dot{r}'/\bar{\dot{r}} \\ p'/\bar{p} \end{pmatrix} = \begin{pmatrix} 0 \\ 0 \\ 0 \\ 0 \end{pmatrix} \tag{A3}$$

The parameter λ is the eigenvalue from the solution to the transient heat equation in the solid. It is defined in Eq. (21). The parameters A, B, n, and n_s are defined in terms of partial differentials of the dependent and independent variables:

$$n = \frac{\bar{p}}{\bar{\dot{r}}}\left(\frac{\partial \dot{r}}{\partial p}\right)_{T_i} \qquad \frac{1}{B} = \frac{\bar{T}_s - T_i}{\bar{\dot{r}}}\left(\frac{\partial \dot{r}}{\partial T_i}\right)_p \tag{A4}$$

$$n_s = \frac{\bar{p}}{\bar{\dot{r}}}\left(\frac{\partial \dot{r}}{\partial p}\right)_{T_s} \qquad A = \frac{\bar{T}_s - T_i}{\bar{\dot{r}}}\left(\frac{\partial \dot{r}}{\partial T_s}\right)_p \tag{A5}$$

The response functions can be calculated by putting Eq. (A3) into row echelon form, using elementary row and column operations[66]:

$$\begin{pmatrix} 1 & 0 & 0 & 0 & -\boldsymbol{R}_{T_i,p} \\ 0 & 1 & 0 & 0 & -\boldsymbol{R}_{T_s,p} \\ 0 & 0 & 1 & 0 & -\boldsymbol{R}_{f_s,p} \\ 0 & 0 & 0 & 1 & -\boldsymbol{R}_{\dot{r},p} \end{pmatrix} \begin{pmatrix} T_i'/(\bar{T}_s - T_i) \\ T_s'/(\bar{T}_s - T_i) \\ f_s'/\bar{f}_s \\ \dot{r}'/\bar{\dot{r}} \\ p'/\bar{p} \end{pmatrix} = \begin{pmatrix} 0 \\ 0 \\ 0 \\ 0 \end{pmatrix} \tag{A6}$$

We can then read the response functions that we need from the right-hand column:

$$\boldsymbol{R}_{\dot{r},p} = \frac{nAB + n_s(\lambda - 1)}{\lambda + A/\lambda - (A+1) + AB} \tag{A7}$$

$$\boldsymbol{R}_{f_s,p} = -\frac{1}{\lambda}\frac{nAB + n_s(\lambda^2 - 1) + B\lambda^2(n - n_s)}{\lambda + A/\lambda - (A+1) + AB} \tag{A8}$$

Acknowledgments

The authors would like to thank Program Monitor Judah Goldwasser of ONR for his support. M.S. graduate Ryo Fuchinoue was responsible for assembling the oscillatory chamber and running the experiments. M.S. students Sinil Chai and Chris Brdar also ran many of the experiments. The authors would especially like to thank William D. O'Brien, of the Department of Electrical and Computer Engineering at the University of Illinois at Urbana–Champaign (UIUC), for his help and expertise in setting up the ultrasound system; Harry S. Hilton, of the Department of Aeronautical and Astronautical Engineering at UIUC, for helpful discussions regarding viscoelasticity and the mechanical properties of propellants; and Robert S. Brown, for providing information concerning the United Technologies Chemical Systems Division rotating valve burner. Experimental data from the T-burner and the magnetic flowmeter were provided by Fred Blomshield at the Naval Air Warfare Center and Michael Micci at Pennsylvania State University, respectively.

References

[1] Ankarswärd, B., "The Hybrid Rocket Engine," *Interavia*, Vol. 19, No. 12, 1964, pp. 1838–1840.

[2] Ho, P. J., "Feasibility Study of the Microwave and the Ultrasonic Techniques on the Continuous Measurement of Solid Propellant Burning Rates," M.S. Thesis, Purdue Univ., West Lafayette, IN, Aug. 1965.

[3] Hale, H. J., "The Demonstration of an Ultrasonic Technique to Measure Solid Propellant Burning Rates Under Actual Combustion Conditions," M.S. Thesis, Virginia Polytechnic Inst., and State Univ., Blacksburg, VA, June 1967.

[4] Wright, W. A., "Ultrasound Thickness Monitoring Technique," *Aerospace Related Technology for Industry*, NASA SP-5075, 1969, pp. 69–72.

[5] Kuentzmann, P., Demarais, J. C., and Cauty, F., "Ultrasonic Measurements of Solid Propellant Burning Rate," *La Recherche Aérospatiale*, Vol. **XX**, No. 1, 1979, pp. 55–72.

[6] Traineau, J. C., and Kuetzmann, P., "Ultrasonic Measurements of Solid Propellant Burning Rates in Nozzleless Rocket Motors," *Journal of Propulsion and Power*, Vol. 2, No. 3, 1986, pp. 215–222.

[7] Cauty, F., "Measurement of Solid Propellant Response Function at Low Frequency by Means of Ultrasonic Method," ONERA, TP 1995-108, Châtillon, France, 1995.

[8] Cauty, F., "Solid-Propellant Combustion Response Function from Direct Measurement Methods–ONERA Experience," *Journal of Propulsion and Power*, Vol. 15, No. 6, 1999, pp. 837–843.

[9] Leahy, J. C., and Jackson, J. W., Jr., "Improvements in the Measurement of Hybrid Rocket Fuel Regression Rate Using Ultrasonic Transducers," AIAA Paper 97-3082, July 1997.

[10] McQuade, W. W., Dauch, F., Moser, M. D., and Fredrick, R., Jr., "Determination of the Ultrasonic Burning Rate Technique Resolution," AIAA Paper 98-3555, July 1998.

[11] Korting, P. A. O. G., and Schöyer, H. F. R., "Determination of the Regression Rate in Solid Fuel Ramjets by Means of the Ultrasonic Pulse Echo Method," *Heat Transfer in Fire and Combustion Systems*, Vol. HTD 45, American Society of Mechanical Engineers, Fairfield, NJ, 1985, pp. 347–353.

[12] Louwers, J., Gadiot, G. M. H. J. L., Versluis, M., Landman, A. J., van der Meer, T. H., and Roekaerts, D., "Measurement of Steady and Non-Steady Regression Rates of Hydrazinium Nitroformate with Ultrasound," International Workshop on Measurement of Thermophysical and Ballistic Properties of Energetic Materials, Politecnico di Milano, Italy, June 1998.

[13] Deepak, D., Jeenu, R., Sridharan, P., and Padmanabhan, M. S., "Determination of Pressure Dependence of Burning Rate in Solid Motors Using Ultrasound Technique," *Journal of Propulsion and Power*, Vol. 14, No. 3, 1998, pp. 290–294.

[14] Korting, P. A. O. G., Schöyer, H. F. R., and Timnat, Y. M., "Advanced Hybrid Rocket Motor Experiments," *Acta Astronautica*, Vol. 15, No. 2, 1987, pp. 97–104.

[15] Fredrick, R. A., Jr., and Traineau, J. C., "Survey of Ultrasonic Instrumentation for Burning Rate Measurement," *JANNAF 36th Combustion Subcommittee Meeting*, CPIA Publ. 691, Vol. 1, Chemical Propulsion Information Agency, Laurel, MD, 1999, pp. 195–216.

[16] Cauty, F., Demarais, J., Erades, C., and Caugant, C., "Internal Insulation and Solid Propellant Behavior Measured by Ultrasonic Method on Solid Rocket Motors," AIAA Paper 97-2994, July 1997.

[17] Dijkstra, F., Korting, P., and van der Berg, R., "Ultrasonic Regression Rate Measurement in Solid Fuel Ramjets," AIAA Paper 90-1963, July 1990.

[18] Traineau, J. C., Prévost, M., and Tarrin, P., "Experimental Low and Medium Frequency Determination of Solid Propellants Pressure-Coupled Response Function," AIAA Paper 94-3043, July 1994.

[19] Salvo, R. D., Frederick, R. A., Jr., and Moser, M. D., "Direct Ultrasonic Measurement of Solid Propellant Combustion Transients," AIAA Paper 99-2223, June 1999.

[20] Cardiff, E. H., Herndon, B., Saretto, S., and Micci, M. M., "Magnetic Flowmeter Measurements of Solid Propellant Combustion Responses,"

JANNAF 36th Combustion Subcommittee Meeting, CPIA Publ. 691, Vol. 1, Chemical Propulsion Information Agency, Laurel, MD, 1999, pp. 587–596.

[21]Culick, F. E. C., "T-Burner Testing of Metallized Solid Propellants," Air Force Rocket Propulsion Lab., AFRPL-TR-74-28, Edwards Air Force Base, CA, Oct. 1974, available from National Technical Information Service, U.S. Department of Commerce, AD/A-001 665.

[22]McLaughlin, K., "A Beginner's Guide to—Wall Thickness Measurement Using Ultrasound," *British Journal of Non-Destructive Testing*, Vol. 31, No. 4, 1989, pp. 196–198.

[23]Papadakis, E. P., "Ultrasonic Velocity and Attenuation: Measurement Methods with Scientific and Industrial Applications," *Physical Acoustics*, edited by W. P. Mason and R. N. Thurston, Vol. 12, Academic Press, New York, 1976, pp. 277–374.

[24]Royer, D., and Casula, O., "A Sensitive Ultrasonic Method for Measuring Transient Motions of a Surface," *Applied Physics Letters*, Vol. 67, No. 22, 1995, pp. 3248–3250.

[25]Lévesque, D., Legros, A., Michel, A., and Piché, L., "High Resolution Ultrasonic Interferometry for Quantitative Nondestructive Characterization of Interfacial Adhesion in Multilayer (Metal/Polymer/Metal) Composites," *Journal of Adhesion Science and Technology*, Vol. 7, No. 7, 1993, pp. 719–741.

[26]Eriksson, H., Börjesson, P. O., Ödling, P., and Holmer, N. G., "A Robust Correlation Receiver for Distance Estimation," *IEEE Transactions on Ultrasonics, Ferroelectrics, and Frequency Control*, Vol. 41, No. 5, 1994, pp. 596–603.

[27]Kinsler, L. E., Frey, A. R., Coppens, A. B., and Sanders, J. V., *Fundamentals of Acoustics*, 3rd ed., Wiley, New York, 1982, pp. 58–60.

[28]Ferry, J. D., *Viscoelastic Properties of Polymers*, 3rd ed., Wiley, New York, 1980.

[29]Duncan, E. J. S., and Brousseau, P., "Comparison of the Uniaxial Tensile Modulus and Dynamic Shear Storage Modulus of a Filled Hydroxy-Terminated Polybutadiene and GAP Propellant," *Journal of Materials Science*, Vol. 31, No. 5, 1996, pp. 1275–1284.

[30]Lighthill, J. M., "Group Velocity," *Journal of Institute of Mathematics and its Applications*, Vol. 1, No. 1, 1965, pp. 1–28.

[31]Kinra, V. K., "Dispersive Wave Propagation in Random Particulate Composites," *Recent Advances in Composites in the United States and Japan*, edited by J. R. Vinson and M. Taya, Vol. STP 864, American Society for Testing and Materials, Philadelphia, 1985, pp. 309–325.

[32]Beltzer, A. I., Bert, C. W., and Striz, A. G., "On Wave Propagation in Random Particulate Composites," *International Journal of Solids and Structures*, Vol. 19, No. 9, 1983, pp. 785–791.

[33]Kim, J. Y., Ih, J. G., and Lee, B. H., "Dispersion of Elastic Waves in Random Particulate Composites," *Journal of the Acoustical Society of America*, Vol. 97, No. 3, 1995, pp. 1380–1388.

[34]Embree, P. M., and O'Brien, W. D., Jr., "Pulsed Doppler Accuracy Assessment Due to Frequency-Dependent Attenuation and Rayleigh Scattering Error Sources," *IEEE Transactions on Biomedical Engineering*, Vol. 37, No. 3, 1990, pp. 322–326.

[35]Carter, G. C., "Time Delay Estimation," *IEEE Transactions on Acoustics, Speech, and Signal Processing*, Vol. ASSP-29, No. 3, 1981, p. 461.

[36]Bendat, J. S., and Persol, A. G., *Random Data Analysis and Measurement Procedures*, 2nd ed., Wiley, New York, 1986, pp. 118–120.

[37]White, P. H., "Cross Correlation in Structural Systems: Dispersion and Nondispersion Waves," *Journal of the Acoustical Society of America*, Vol. 45, No. 5, 1967, pp. 1118–1128.

[38]Boucher, R. E., and Hassab, J. C., "Analysis of Discrete Implementation of Generalized Cross Correlator," *IEEE Transactions of Acoustics, Speech, and Signal Processing*, Vol. ASSP-29, No. 3, 1981, pp. 609–611.

[39]Moddemeijer, R., "On the Determination of the Position of Extrema of Sampled Correlators," *IEEE Transactions of Signal Processing*, Vol. 39, No. 1, 1991, pp. 216–219.

[40]Paradis, L., Serruys, Y., and Saglio, R., "Ultrasonic Signal Processing for Thickness Measurements and Detection of Near-Surface Defects," *Materials Evaluation*, Vol. 44, No. 11, 1986, pp. 1344–1349.

[41]Kemerait, R. C., and Childers, D. G., "Signal Detection and Extraction by Cepstrum Techniques," *IEEE Transactions on Information Theory*, Vol. IT-18, No. 6, 1972, pp. 745–759.

[42]Hassab, J. C., and Boucher, R., "A Probabilistic Analysis of Time Delay Extraction by the Cepstrum in Stationary Gaussian Noise," *IEEE Transactions on Information Theory*, Vol. IT-22, No. 4, 1976, pp. 444–454.

[43]Oppenheim, A. V., and Schafer, R. W., *Discrete-Time Signal Processing*, Prentice–Hall, Englewood Cliffs, NJ, 1989, pp. 768–771.

[44]Etter, D. M., and Stearns, S. D., "Adaptive Estimation of Time Delays in Sampled Data Systems," *IEEE Transactions on Acoustics, Speech, and Signal Processing*, Vol. ASSP-29, No. 3, 1981, pp. 582–587.

[45]Jacovitti, G., and Scarano, G., "Discrete Time Techniques for Time Delay Estimation," *IEEE Transactions on Signal Processing*, Vol. 41, No. 2, 1993, pp. 525–533.

[46]Grennberg, A., and Sandell, M., "Estimation of Subsample Time Delay Differences in Narrowband Ultrasonic Echoes Using the Hilbert Transform Correlation," *IEEE Transactions on Ultrasonics, Ferroelectrics, and Frequency Control*, Vol. 41, No. 5, 1994, pp. 588–595.

[47]Culick, F. E. C., "A Review of Calculations for Unsteady Burning of Solid Propellant," *AIAA Journal*, Vol. 6, No. 12, 1968, pp. 2241–2255.

[48]Son, S. F., and Brewster, M. Q., "Linear Burning Rate Dynamics of Solids Subjected to Pressure or External Radiant Heat Flux Oscillations," *Journal of Propulsion and Power*, Vol. 9, No. 2, 1993, pp. 222–232.

[49]Murphy, J. J., and Krier, H., "Linear Pressure Coupled Frequency Response of Heterogeneous Solid Propellants," *Twenty-seventh Symposium (International) on Combustion*, The Combustion Institute, Pittsburgh, PA, 1998, pp. 2343–2350.

[50]Özüpek, Ş., and Becker, E. B., "Constitutive Equations for Solid Propellants," *Journal of Engineering Materials and Technology*, Vol. 119, No. 2, 1997, pp. 125–132.

[51]Christensen, R. M., *Theory of Viscoelasticity, an Introduction*, 2nd ed., Academic Press, New York, 1982.

[52]Adicoff, A., and Lepie, A. H., "Effect of Tensile Strain on the Use of the WLF Equation," *Journal of Applied Polymer Science*, Vol. 14, No. 4, 1970, pp. 953–966.

[53]Droste, D. H., and Dibenedetto, A. T., "The Glass Transition Temperature of Filled Polymers and its Effect on their Physical Properties," *Journal of Applied Polymer Science*, Vol. 13, 1969, pp. 2149–2168.

[54]Stacer, R. G., Husband, D. M., and Stacer, H. L., "Viscoelastic Response and Adhesion Properties of Highly Filled Elastomers," *Rubber Chemistry and Technology*, Vol. 60, No. 2, 1987, pp. 227–244.

[55]Stacer, R. G., and Husband, D. M., "Small Deformation Viscoelastic Response of Gum and Highly Filled Elastomers," *Rheologica Acta*, Vol. 29, No. 2, 1990, pp. 152–162.

[56]Mench, M. M., Kuo, K. K., and Lu, Y. C., "Characterization of Burning Rate, Temperature Sensitivity and Stability Behavior of AP-Based Composite Propellants and a Comparison of Thermal Behavior of Ultra-fine Aluminum (Alex) Made from Plasma Explosion Process with Regular Aluminum Powders," Office of Naval Research, Mechanics Div., Final Rept. ONR Contract N00014-96-1-0785, Arlington, VA, Sept. 1997.

[57]Zarko, V. E., and Kuo, K. K., "Critical Review of Methods for Regression Rate Measurements of Condensed Phase Systems," *Non-Intrusive Combustion Diagnostics*, edited by K. K. Kuo and T. P. Parr, Begell House, New York, 1994, pp. 600–623.

[58]Moser, M. D., Dauch, F., and McQuade, W. W., "Surface Roughness Effects on Ultrasonic Burning Rate Measurements," *Proceedings of the 33rd ASME National Heat Transfer Conference*, Paper No. HTD 99-285, American Society of Mechanical Engineers, Fairfield, NJ, 1999.

[59]Brown, R. S., Erickson, J. E., and Babcock, W. R., "Combustion Response Function Measurements by the Rotating Valve Method," *AIAA Journal*, Vol. 12, No. 11, 1974, pp. 1502–1510.

[60]Brown, R. S., "Development and Evaluation of Rotating Valve Combustion Response Test Technique," Air Force Rocket Propulsion Lab., AFRPL-TR-76-72, Edwards Air Force Base, CA, Oct. 1976.

[61]Fuchinoue, R., "Development of the Oscillatory Burner to Measure the Pressure-Coupled Response Function," M.S. Thesis, Dept. of Mechanical and Industrial Engineering, Univ. of Illinois, Urbana–Champaign, IL, Aug. 1999.

[62]Murphy, J. J., "Unsteady Solid Propellant Combustion: Theory and Experiment," Ph.D. Dissertation, Dept. of Mechanical and Industrial Engineering, Univ. of Illinois, Urbana–Champaign, IL. Aug. 2000.

[63]Zanotti, C., Volpi, A., Bianchessi, M., and Luca, L. D., "Measuring Thermodynamic Properties of Burning Propellants," *Nonsteady Burning and Combustion Stability of Solid Propellants*, edited by L. De Luca, E. W. Price, and M. Summerfield, Vol. 143, Progress in Astronautics and Aeronautics, AIAA, Washington, DC, 1992, pp. 145–196.

[64]Cauty, F., Comas, P., Vuillot, F., and Micci, M. M., "Magnetic Flow Meter Measurement of Solid Propellant Pressure-Coupled Responses Using Acoustic Analysis," *Journal of Propulsion and Power*, Vol. 12, No. 2, 1996, pp. 436–438.

[65]Murphy, J. J., "Modeling of the Linear Burning Rate Response of Solid Propellants to Pressure Oscillations," M.S. Thesis, Dept. of Mechanical and Industrial Engineering, Univ. of Illinois, Urbana–Champaign, IL, Jan. 1998.

[66]Friedberg, S. H., Insel, A. J., and Spence, L. E., *Linear Algebra*, 2nd ed., Prentice–Hall, Englewood Cliffs, NJ, 1989, pp. 163–167.